A Local Field Study of a Water-Immersed Microwave Antenna Array for Medical Imagery and Therapy

THEODORE C. GUO, SENIOR MEMBER, IEEE, WENDY W. GUO, SENIOR MEMBER, IEEE, AND LAWRENCE EDWIN LARSEN, SENIOR MEMBER, IEEE

Abstract—**A water-immersed microwave array system for medical imaging is described, and a theoretical analysis of its local field pattern is presented. The theoretical study also applies to similar systems for medical therapy purposes. It is shown that, using a technique of phase and amplitude conjugations, a satisfactory three-dimensional focusing for targets located in the neighborhood of the array may be achieved. The focusing resolutions for transverse and longitudinal directions are approximately $\lambda/2$ and λ, respectively, where λ is the wavelength in the dielectric. By increasing the element spacing of the array, the resolutions can be as good as 5.3 and 11.7 mm, respectively, at the operating frequency of 3 GHz.**

I. Introduction

THE DESIRABILITY of using microwaves for medical diagnosis and therapy has been studied by a number of researchers [1]–[11]. Some problems involved include: 1) low resolution at frequencies below 10 GHz (unless an impractically large antenna aperture is employed) and excessive attenuation at higher frequencies [12]; 2) complication in signal processing caused by multipath propagation exterior to the target [13]; 3) large reflection of the incident energy at the air-tissue interface [14]; and 4) for the therapeutic applications, difficulty in producing localized heating at internal organs due to the inhomogeneous dielectric profile between the applicator and the target organ. Except for the last item, these problems can be simultaneously resolved by submerging both transmitting and receiving antennas, as well as the biological subject, in water. Indeed, the large value of the dielectric constant of water, which is 76.7 at 3 GHz, reduces the wavelength of the radiation by a factor of 8.8 ($\sqrt{76.7}$) and thereby increases the resolution by about the same factor. Also, the high propagation loss of microwaves in water eliminates many sources of multipath. Furthermore, as water is the primary composition of most biological materials, the energy coupling into the target is greatly improved due to the impedance matching at the water–target interface.

Manuscript received October 12, 1983; revised March 8, 1984. This work was supported in part by the Walter Reed Army Institute of Research through the U.S. Army Medical R&D Command under the U.S. Naval Sea Systems Command Contract N00024-83-C-5301.

T. C. Guo and W. W. Guo are with the John Hopkins University Applied Physics Laboratory, Laurel, MD 20707.

L. E. Larsen is with the Department of Microwave Research, Walter Reed Army Institute of Research, Washington, DC 20012.

There remains another difficulty in water-coupled imaging and therapy: the high attenuation of radiation in water inescapably reduces the incident radiation on the target and the desired signal to the receiving antenna. In order to increase the radiation level, to achieve higher resolution, to acquire data at higher speed, and to obtain three-dimensional focusing control, a large antenna array with phase and amplitude control on each element must be used. Still, the high attenuation in water requires that the target be close to the transmitting antenna and, in the case of microwave imaging, also close to the receiving antenna. Indeed, the field at the target is effectively a local field of the radiation sources. Thus, Fraunhofer and Fresnel diffraction, which is commonly used in calculating the field patterns of antenna arrays, cannot be applied.

In this paper, a method similar to the local field optics of crystal lattices is described. It is shown that, using both phase and amplitude conjugations on each element of the antenna array, one may achieve resolution for three-dimensional focusing. These results may be employed for imaging and interrogation of biological targets as well as for application and control of microwave power for therapeutic use. The phase and amplitude conjugations referred to constitute a method of applying the proper phase and amplitude distributions (tapers) to the elements of the transmitting or receiving array to compensate for the propagation path differences and to achieve focusing in the local area of the array (see (27)).

All input data used in this paper correspond to the previously described microwave imagery system at the Walter Reed Army Institute of Research [2],[3],[6]–[8]. A brief description of the system is given in the next section; similar systems may also be made applicable for the therapeutic purpose. Theoretical derivation of the local field formula is summarized in Section III, followed by discussions of the calculated results in Section IV.

II. Description of the System

The system is composed of two antenna arrays, one for transmission and another for reception, submerged in a cylindrical water container of about 3 ft in diameter and 3 ft high. Both antenna arrays are of hexagonal shape with

0018-9480/84/0800-0844$01.00 ©1984 IEEE

127 elements in a brick-staggered arrangement, corresponding to a planar lattice with one lattice vector at 59° from another and 0.97 times the length (Fig. 1(a)). Each element is a 4×7-mm degenerate ellipse waveguide-to-coaxial adapter, which has, at an axial distance of 5 cm or farther, an underwater field pattern in the forward direction similar to that of a dipole field. The two antennas are mounted in adjustable frames, facing each other. The target is to be placed between the two antennas. The axial distance between the antennas and the target may be adjusted from as close as 5 cm to a distance of about 35 cm. Other engineering details may be found in [3]; some of the specifications may still be modified as the theoretical and experimental studies continue to progress.

In order to compensate for the differences of the distance from each of the elements to the target, a method of phase and amplitude conjugations is used. That is, a factor which includes both phase and amplitude is applied to each element depending on its distance to a certain point of the target (the focal point). For imagery purpose, instead of applying the conjugations to the transmitting elements, which would require RF phase shifters, the conjugations are applied to the receiving elements in the form of off-line data processing, i.e., by multiplying the received complex field amplitude in each element by a complex factor corresponding to the phase and amplitude conjugations for a measured omnidirectional source. On the other hand, the phasing of the emitting array is designed to produce a near plane-wave, or, sequentially overlapping subarrays, to provide the ability to illuminate selected areas of the target. In therapeutic applications, an active conjugation approach that applied to the transmitting elements will be necessary.

The phase and amplitude conjugation technique produces a self-focusing array. That is to say, the array's element-to-element variations in phase center, insertion loss, etc. become the data needed for focusing when a defined source illuminates the array elements and separate measurements of scattering parameter S_{21} [15] are made to each element. The same array may be used for imaging and heating. The key idea is a method of hyperthermia controlled by imaging changes in the complex permittivity due to microwave heating. The control and heating functions can be temporally interlaced during the course of therapy. In the case of S_{11} imagery, a central subarray serves as a low-power illuminator, while the remaining elements serve as receivers with diplexer protection. In the case of S_{21} imagery, the array is used as a receiver with diplexer protection, but an additional illuminator is needed.

In order to describe the application of this technique to a water-coupled microwave imaging system, a brief digression into the design of a multiplex receiver is necessary. The receiver consists of 127 open-ended waveguide elements (degenerate ellipse in transverse section) each with a shorted feed for coax-to-waveguide adaptation. The 127 coax lines are routed to 6P1T diode switches in a three-tier reverse corporate power divider network. This network provides the switching to connect each receiver array element to a harmonic converter. Two low-noise amplifiers of 20-dB gain are inserted under operator selection prior to the harmonic converter to compensate for path losses through the coupling medium. The local oscillator for the harmonic converter is derived via a directional coupler from a digital synthesizer which serves as the signal source for the transmitting array. The RF port of the harmonic converter is attached to each element of the receiver array via the switch matrix. The IF port returns the down-converted receiver signal to a complex ratiometer which compares another sample of the transmitted signal with the IF signal from the receiver.

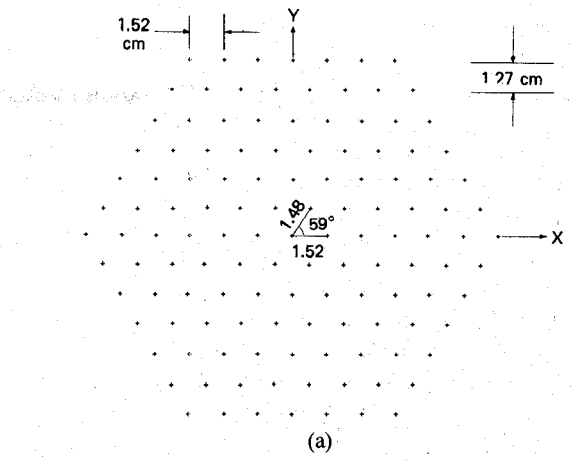

(a)

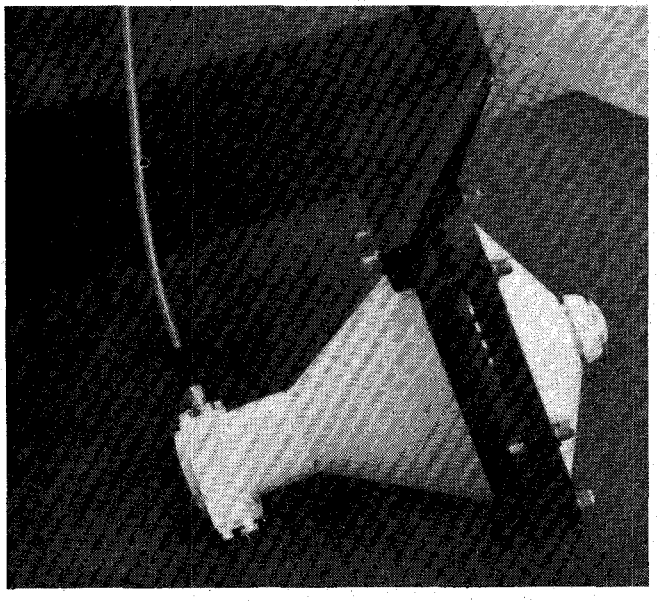

(b)

Fig. 1. (a) The planar array of 127 dipole elements. (b) A water-immersed lens antenna for receiver calibration is shown. This derived the measured data for phase and amplitude conjugations to accomplish three-dimensional focusing.

The amplitude and phase conjugation, therefore, includes not only element-to-element variations in the array geometry, but also path-length and insertion-loss variations in the switch matrix enroute to the harmonic converter. The complex ratiometer provides this measurement by estimating S_{21} for each element over the entire RF signal

path from the source to the RF port of the harmonic converter.

The source used for the S_{21} measurement should ideally consist of a 2π-sr omnidirectional radiator. One realization of such a calibration source is shown in Fig. 1(b). This design is based upon a dielectric lens. It provides a 3-dB beamwidth of 130° in azimuth and in elevation. The amplitude for each element and its path to the harmonic converter for a given position of the calibration source provides the amplitude taper needed to compensate for path losses through the coupling medium and insertion losses in the switch matrix. That is, the needed amplitude taper is the inverse of the measured amplitude taper for that position of the calibration source. The needed phase taper to ensure coherent addition at the portion of the calibration source is the conjugate of each measured phase. All focal spot positions are provided by translation of the calibration source.

The calibration data set derived as described above is then applied to the S_{21} measurements in the presence of a target for each element for each focal point. In this way, the forward scattered fields are scanned by a sensitive volume element. The receiver array focusing takes place off-line. The array is focused only in the coupling medium, not in the target. The forward scattered fields from the target are differenced from the beam pattern of the illuminator recorded at the same plane in the absence of the target.

III. The Local Field Formula

In this section, the formula for the electromagnetic field in the neighborhood of a lattice radiation source is derived. The formula will be used to calculate the field pattern of the antenna array and the beam characteristics. The antenna array is treated as a localized distribution of charge and current in a lattice structure. The following three assumptions are made:

1) If d_l and d_t represent, respectively, the longitudinal and transverse dimensions of each array element with respect to the direction of the point of observation, and r_n the distance from the nth element to the observation point, it is assumed that, for every element, the following magnitude comparisons are valid:

$$r_n \gg d_l \quad \text{and} \quad d_t, \qquad \lambda \gg d_l, \qquad \lambda \gg d_t^2/r_n \tag{1}$$

where λ is the wavelength of the microwave signal in water. Under this assumption, the field due to each radiating element may be approached by the dipole approximation.

2) Mutual couplings between the radiating elements are included in the local field formula to the extent that the effect of all couplings is assumed to be identical in every element. In other words, the difference between the peripheral elements and the interior elements with regard to the effect of mutual coupling is assumed to be negligible.

3) Mutual coupling between the radiating elements is linear with respect to the phase and amplitude of the power input to the elements. Measured mutual coupling using a Hewlett Packard 8542C Automated Network Analyzer (ANA) proved this assumption to be true and demonstrated that mutual coupling is $\leqslant -80$ dB.

It is remarked that assumption 1) is of a quantitative nature, in the sense that its degree of satisfaction depends on the degree of quantitative precision needed for the field pattern. Although the physical size of each array element is about half the wavelength, it is the actual current distribution that determines the size of the source. Our calibration measurements show that the field of each individual array element resembles that of a dipole, indicating that this assumption is valid for the system. It will be made clear where this assumption, as well as the other two assumptions, enter into the derivation, so that the percentage error of the derived quantities may be determined.

To derive the local field formula, consider a localized charge density ρ and current density $\vec{J}$ distributed in a space region V. For an antenna in a free space, V indicates the space occupied by the antenna array, as well as its accessories. Without losing any generality, monochromatic time variation is assumed, so that

$$\rho(\vec{x}, t) = \rho(\vec{x}) e^{-i\omega t}$$

and

$$\vec{J}(\vec{x}, t) = \vec{J}(\vec{x}) e^{-i\omega t}. \tag{2}$$

Accordingly, all other field quantities resulting from ρ and $\vec{J}$ also vary with time monochromatically. Any other time variation can always be obtained by superposition of monochromatic waves. From Maxwell's equation, the vector potential at any point outside of V is given by, in the Gaussian system of units [16]

$$\vec{A}(\vec{x}) = \int_V \frac{1}{c} \vec{J}(\vec{x}') \frac{\exp ik|\vec{x} - \vec{x}'|}{|\vec{x} - \vec{x}'|} d\vec{x}' \tag{3}$$

from which one obtains the magnetic induction $\vec{B}$ and electric field strength $\vec{E}$

$$\vec{B}(\vec{x}) = \nabla \times \vec{A}(\vec{x}) \tag{4}$$

and

$$\vec{E}(\vec{x}) = \frac{1}{k} \nabla \times \vec{B}(\vec{x}) \tag{5}$$

where k is the magnitude of the wave vector in the medium. For water, k is a complex quantity $k_1 + ik_2$ where k_1 is equal to 2π times the inverse of the wavelength and k_2 is the inverse of the distance over which the field is attenuated by a factor of $e = 2.72$ (equivalent to a power loss of 8.7 dB). At an operating frequency of 3 GHz in water, the values of k_1 and k_2 are

$$k_1 = 5.5 \text{ cm}^{-1} \quad \text{and} \quad k_2 = 0.44 \text{ cm}^{-1}. \tag{6}$$

The current–charge volume V is divided into a number of subvolumes, each denoted by V_n, which represents the space occupied by the nth radiating element. Let $\vec{x}_n$ be the center of V_n and denote by $\vec{J}_n$ and ρ_n, respectively, the current density and the charge density in V_n with respect to

its center, then

$$\vec{J}_n(\vec{x}) = \vec{J}(\vec{x}+\vec{x}_n) \quad \text{and} \quad \rho_n(\vec{x}) = \rho(\vec{x}+\vec{x}_n). \quad (7)$$

Clearly, (3) may also be written as

$$\vec{A}(\vec{x}) = \sum_{n=1}^{N} \int_{V_n} \frac{1}{c}\vec{J}(\vec{x}) \frac{\exp(ik|\vec{x}-\vec{x}'|)}{|\vec{x}-\vec{x}'|}\, d\vec{x}'. \quad (8)$$

Making the change of variable $\vec{x}' \to \vec{x}_n + \vec{x}'$, where the new $\vec{x}'$ is a vector from the center of each element to the volume $d\vec{x}'$, which is identical for every n and thus may simply be regarded as a vector in V_1, using (7), (8) becomes

$$\vec{A}(\vec{x}) = \sum_{n=1}^{N} \int_{V_1} \frac{1}{c}\vec{J}_n(\vec{x}') \frac{\exp ik|(\vec{x}-\vec{x}_n)-\vec{x}'|}{|(\vec{x}-\vec{x}_n)-\vec{x}'|}\, d\vec{x}'. \quad (9)$$

Note that each integral in the right-hand side of (9) is the same as that in (3), except that $\vec{x}$ is replaced by $\vec{x}-\vec{x}_n$ and the space of integration is over only the center element V_1 instead of the entire array, V. Therefore, even though the observation point is in the neighborhood of the array, as long as $|\vec{x}-\vec{x}_n| = r_n$ is much greater than the size of each array element d, one may expand the integrand in (9) in powers of $\vec{x}'/r_n$ (note that $|\vec{x}'| \leqslant d$).

So, denote by $\vec{x}_l'$ and $\vec{x}_t'$, respectively, the longitudinal and transverse components of $\vec{x}'$, i.e., the projections of $\vec{x}'$ in the directions parallel and perpendicular to $\vec{x}-\vec{x}_n$, then

$$\vec{x}_l' = \frac{1}{r_n^2}\left[\vec{x}'\cdot(\vec{x}-\vec{x}_n)\right](\vec{x}-\vec{x}_n) \quad (10)$$

and

$$\vec{x}_t' = -\frac{1}{r_n^2}\left[\vec{x}'\times(\vec{x}-\vec{x}_n)\right]\times(\vec{x}-\vec{x}_n). \quad (11)$$

Define

$$x_l' = |\vec{x}_l'|, \qquad x_t' = |\vec{x}_t'|. \quad (12)$$

Then one has the identity

$$|\vec{x}-\vec{x}_n-\vec{x}'| = \left[(r_n - x_l')^2 + x_t'^2\right]^{1/2}$$

or

$$|\vec{x}-\vec{x}_n-\vec{x}'| = r_n\left(1-\frac{x_l'}{r_n}\right)\left[1+\frac{(x_t'/r_n)^2}{(1-x_l'/r_n)^2}\right]^{1/2}. \quad (13)$$

Under assumption 1), x_l'/r_n and x_t'/r_n are both small quantities. Then, expand $|\vec{x}-\vec{x}_n-\vec{x}'|$ and other functions of it in powers of x_l'/r_n and x_t'/r_n and the following series results:

$$k|\vec{x}-\vec{x}_n-\vec{x}'| = kr_n\left\{1-\frac{x_l'}{r_n}+\frac{1}{2}\left(\frac{x_l'}{r_n}\right)^2-\frac{1}{2}\left(\frac{x_l'}{r_n}\right)\left(\frac{x_t'}{r_n}\right)^2 + \left(\frac{x_t'}{r_n}\right)^2 0\left[\left(\frac{x_l'}{r_n}\right)^2, \left(\frac{x_t'}{r_n}\right)^2\right]\right\} \quad (14)$$

and

$$\frac{1}{|\vec{x}-\vec{x}_n-\vec{x}'|} = \frac{1}{r_n}\left\{1+\frac{x_l'}{r_n}+\left(\frac{x_l'}{r_n}\right)^2-\frac{1}{2}\left(\frac{x_t'}{r_n}\right)^2 + \left(\frac{x_l'}{r_n}\right)0\left[\left(\frac{x_l'}{r_n}\right)^2, \left(\frac{x_t'}{r_n}\right)^2\right]+0\left[\left(\frac{x_t'}{r_n}\right)^4\right]\right\}. \quad (15)$$

As to the factor $\exp(ik|\vec{x}-\vec{x}_n-\vec{x}'|)$, its expansion depends not only on the relative magnitude of r_n and d, but also on the magnitudes of kr_n and kd. If the real part of kd is small, which is valid under assumption 1), then, except for the first term, every term on the right-hand side of (14) is much smaller than 1. The exponential of the series then gives

$$\exp(ik|\vec{x}-\vec{x}_n-\vec{x}'|) = \exp(ikr_n)(1-ikx_l'+\cdots). \quad (16)$$

Combining this expansion with (15), the integrand of (9) becomes

$$\frac{1}{c}J_n(\vec{x}')\frac{\exp(ik|\vec{x}-\vec{x}_n-\vec{x}'|)}{|\vec{x}-\vec{x}_n-\vec{x}'|} = \frac{1}{c}\frac{\exp(ikr_n)}{r_n}J_n(\vec{x}')\left\{1+\frac{x_l'}{r_n}-ikx_l'+\cdots\right\}. \quad (17)$$

Substituting the leading term on the right-hand side of (17) into (9), an approximation for the vector potential is obtained as

$$\vec{A}(\vec{x}) = \sum_{n=1}^{N}\frac{1}{c}\frac{\exp(ikr_n)}{r_n}\int_{V_1}\vec{J}_n(\vec{x}')\, d\vec{x}'. \quad (18)$$

It can be shown that the integral in the right-hand side is proportional to the total dipole moment $\vec{p}_n$ of the array element v_n

$$\vec{P}_n = \frac{i}{ck}\int_{V_1}\vec{J}_n(\vec{x}')\, d\vec{x}' = \frac{i}{ck}\int_{V_n}J(\vec{x}')\, d\vec{x}' \quad (19)$$

where the dipole p_n is defined as the moment of the charge distribution of the nth radiating element with respect to its center

$$\vec{p}_n = \int_{V_1}\vec{x}'\rho(\vec{x}')\, d\vec{x}'. \quad (20)$$

Therefore, the vector potential may also be written as

$$\vec{A}(\vec{x}) = -ik\sum_{n=1}^{N}\vec{p}_n\frac{\exp(-ik|\vec{x}-\vec{x}_n|)}{|\vec{x}-\vec{x}_n|} \quad (21)$$

which is the field due to N radiating dipoles.

Assumptions 2) and 3) are now applied to (21). Noting that all elements have the same geometry, the only factors that could contribute to different values of $\vec{p}_n$ for different elements are the input power and phase and the differences in the current–charge distributions due to mutual coupling. Under assumption 2), the last factor is assumed to be negligible, and, under assumption 3), $\vec{p}_n$ must be proportional to the input phase and amplitude factor. Therefore, $\vec{p}I_nC_n$ may be substituted for $\vec{p}_n$ in (21), where $\vec{p}$ is the

dipole moment for each radiating element at a certain standard input, I_n is the illumination factor for the nth element, and C_n is a complex factor representing the phase and amplitude conjugations. I_n is used as a controlling factor to modify the main-beam shape. Equation (21) then becomes

$$\vec{A}(\vec{x}) = -ik\vec{p}\sum_{n=1}^{N} I_n C_n \frac{\exp(ik/|\vec{x}-\vec{x}_n|)}{|\vec{x}-\vec{x}_n|}. \quad (22)$$

The electric and magnetic fields may be obtained from (22) by applying (4) and (5) on $\vec{A}(\vec{x})$. Again, applying assumption 1), the results are

$$\vec{B}(\vec{x}) = -k^2\vec{p}\times\sum_{n=1}^{N} I_n C_n \frac{\vec{x}-\vec{x}_n}{|\vec{x}-\vec{x}_n|}\frac{\exp(ik|\vec{x}-\vec{x}_n|)}{|\vec{x}-\vec{x}_n|} \quad (23)$$

and

$$\vec{E}(\vec{x}) = -k^2\sum_{n=1}^{N} I_n C_n\left(\vec{p}\times\frac{\vec{x}-\vec{x}_n}{|\vec{x}-\vec{x}_n|}\right)\times\frac{\vec{x}-\vec{x}_n}{|\vec{x}-\vec{x}_n|}\frac{\exp(ik|\vec{x}-\vec{x}_n|)}{|\vec{x}-\vec{x}_n|}. \quad (24)$$

To focus the main beam at the point $\vec{x}_f$, the conjugation factor C_n is given by

$$C_n = |\vec{x}_f-\vec{x}_n|\exp(-ik|\vec{x}_f-\vec{x}_n|). \quad (25)$$

Noting that k is a complex number, the exponential factor in the above equation includes a phase factor and a factor to compensate for the absorption by the propagation medium, the factor $|\vec{x}_f-\vec{x}_n|$ in front of the exponential is to compensate for the inverse-square loss.

The definition of the quantities in (22) and (25) are summarized below:

- $\vec{A}$ the vector potential, in the Gaussian system of units,
- $\vec{B}$ the magnetic induction, in the Gaussian system of units,
- C_n the complex number representing the phase and amplitude conjugation for the nth radiating element,
- $\vec{E}$ the electric-field intensity, in the Gaussian system of units,
- I_n the illumination factor for the nth element; this factor is used to control the beam shape,
- k the complex number representing the magnitude of the wave vector of the radiation in water; the values of its real and imaginary part for a 3-GHz radiation are given in (6),
- n a subscript denoting the nth radiating element,
- N the total number of radiating element in the array,
- $\vec{p}$ the dipole moment of each radiating element at a standard phase and amplitude input (i.e., for I_n and C_n being unity), in the Gaussian system of units,
- $\vec{x}$ the vector representing the observation point with respect to the center of the array,
- $\vec{x}_f$ the desired focal point of the main beam,
- $\vec{x}_n$ the vector representing the center of the nth radiating element with respect to the center of the array.

Note that, for a planar array of $N\times M$ radiating dipole elements, (22) and (25) yield

$$\vec{A}(\vec{x}) = -ik\vec{p}\sum_{n=1}^{N}\sum_{m=1}^{M} I_{nm}C_{nm}\frac{e^{ik|\vec{x}-\vec{x}_{nm}|}}{|\vec{x}-\vec{x}_{nm}|} \quad (26)$$

and

$$C_{nm} = |\vec{x}_f-\vec{x}_{nm}|\exp(-ik|\vec{x}_f-\vec{x}_{nm}|) \quad (27)$$

and $\vec{B}$ and $\vec{E}$ will be changed accordingly.

IV. Resolution and 3-D Focusing

Using (22) and (27), the electromagnetic fields may be calculated and the field characteristics may be obtained. This section presents some results and briefly discusses their significance. Only the absolute value of vector potential and the corresponding field characteristics are presented here. The structure of the array lattice is illustrated in Fig. 1(a), and the equations used are (26), (27), and (6), with illumination factor $I_{nm}=1$, and polarization taken to be in y direction. In all the figures, the plane of the array is taken to be the xy-plane and the z-axis is perpendicular to the array plane and pointing to the forward direction. In the following discussion and in all figures, the phrase "mainbeam" is used in reference to field characteristics of the three-dimensional focal region. Fig. 2(a)–(e) shows various field patterns with different interelement spacings in the transverse plane at an axial distance of 7 cm, which is also the axial distance of the desired focal point. Similarly, Fig. 3(a)–(e) is the longitudinal field patterns at different interelement spacings and focal points. The corresponding 3-dB full-mainbeam width is given on each figure. Note that Figs. 2(b), (c) and 3(b), (c) are for the array with lattice structure shown in Fig. 1(a). Fig. 2(d) and (e) shows arrays that are similar to the one shown in Fig. 1(a), except with different lattice spacings. Figs. 2(a) and 3(a) are for the same size array as shown in Fig. 1(a), but with 419 instead of 127 elements. Figs. 4 and 5 are the corresponding pictures of Figs. 2 and 3, and plotted in isodecibel field contours. For easy comparison, the beam characteristics of these figures are tabulated in Table I. It is clearly seen that, with larger element spacing, the 3-dB beamwidth becomes narrower. Also, the deviation from the predicted focal point becomes less. However, the grating lobes become more of a problem. It also shows that the array size plays a more important role than the number of elements of the array in beamwidth reduction. Resolutions of $\frac{1}{2}\lambda$ in the transverse direction and 1λ in the longitudinal direction can be achieved with the use of phase and amplitude conjugation. Note also that the peaks along $z=2.5$ cm shown in Fig. 3(a)–(e) and Fig. 5(a)–(e) are due to the single element that is closest to each of these peaks. As the range becomes so close to an individual element, the coherent addition from other elements is negligible in comparison. As long as the target is not too close to the array, these peaks will not cause any problem for actual applications in microwave imagery or microwave therapy.

Summarizing the above results, the following conclusions may be drawn:

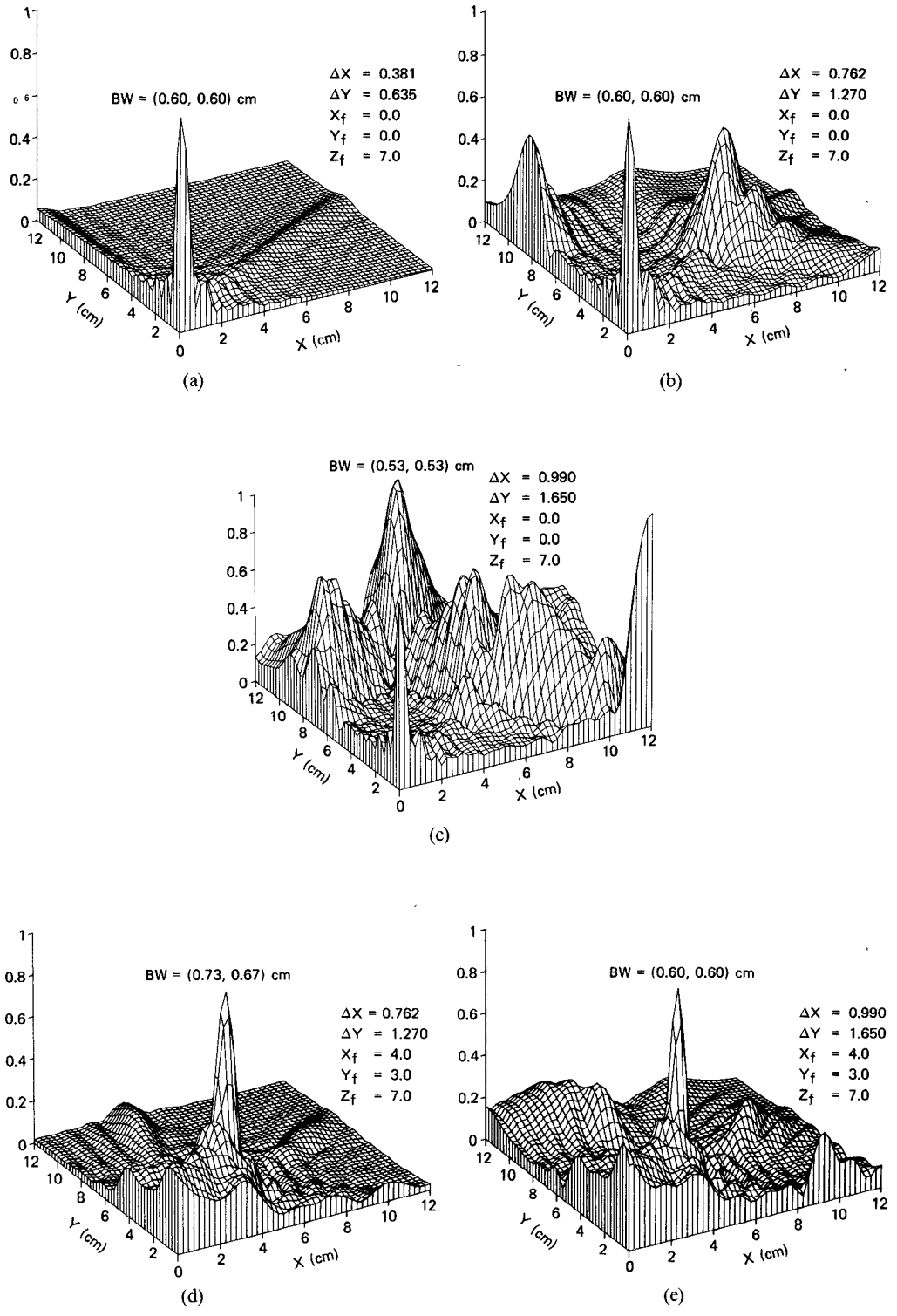

Fig. 2. Relative amplitude surface for constant $Z_f = 7.0$.

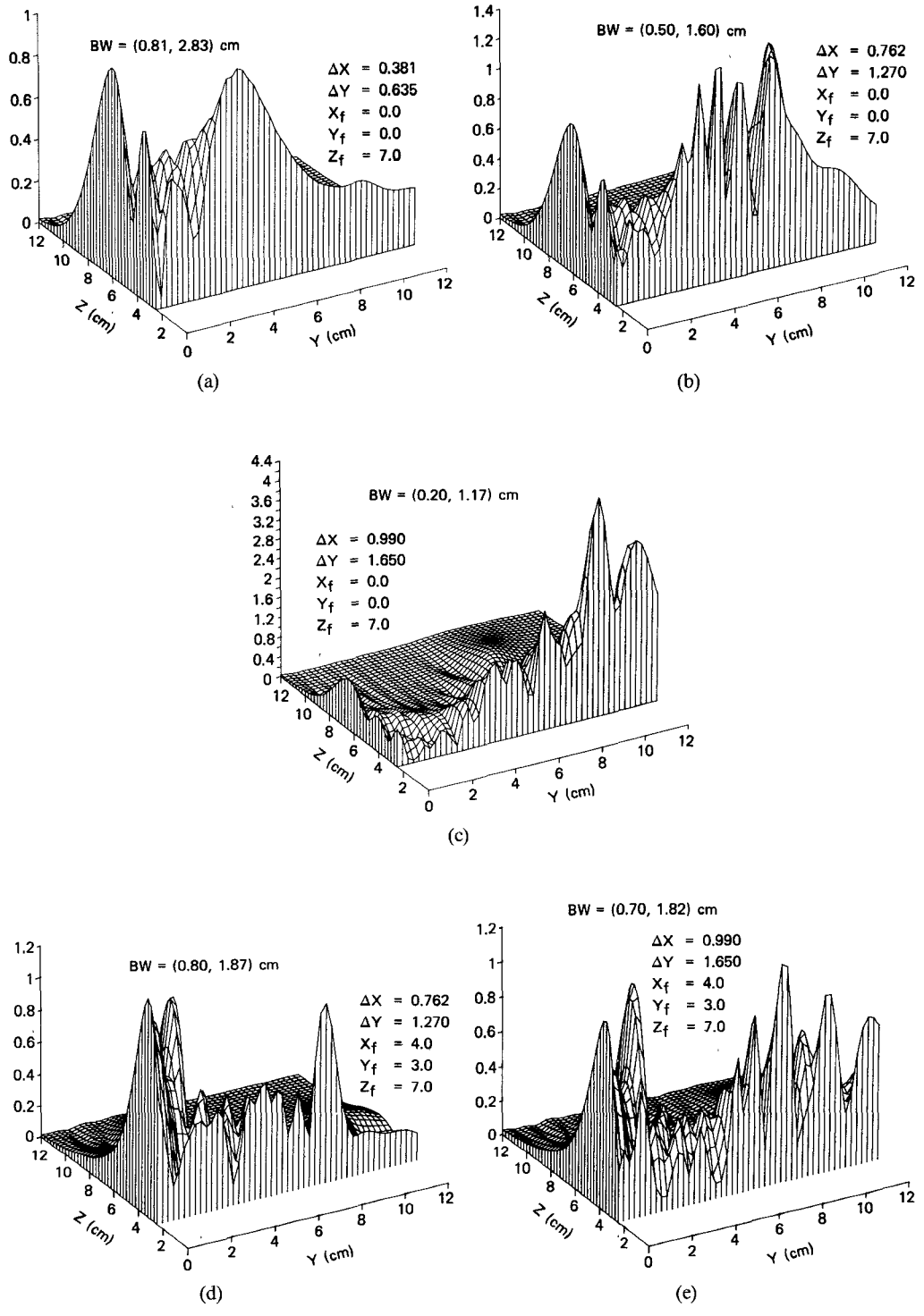

Fig. 3. Relative amplitude surface for constant X_f.

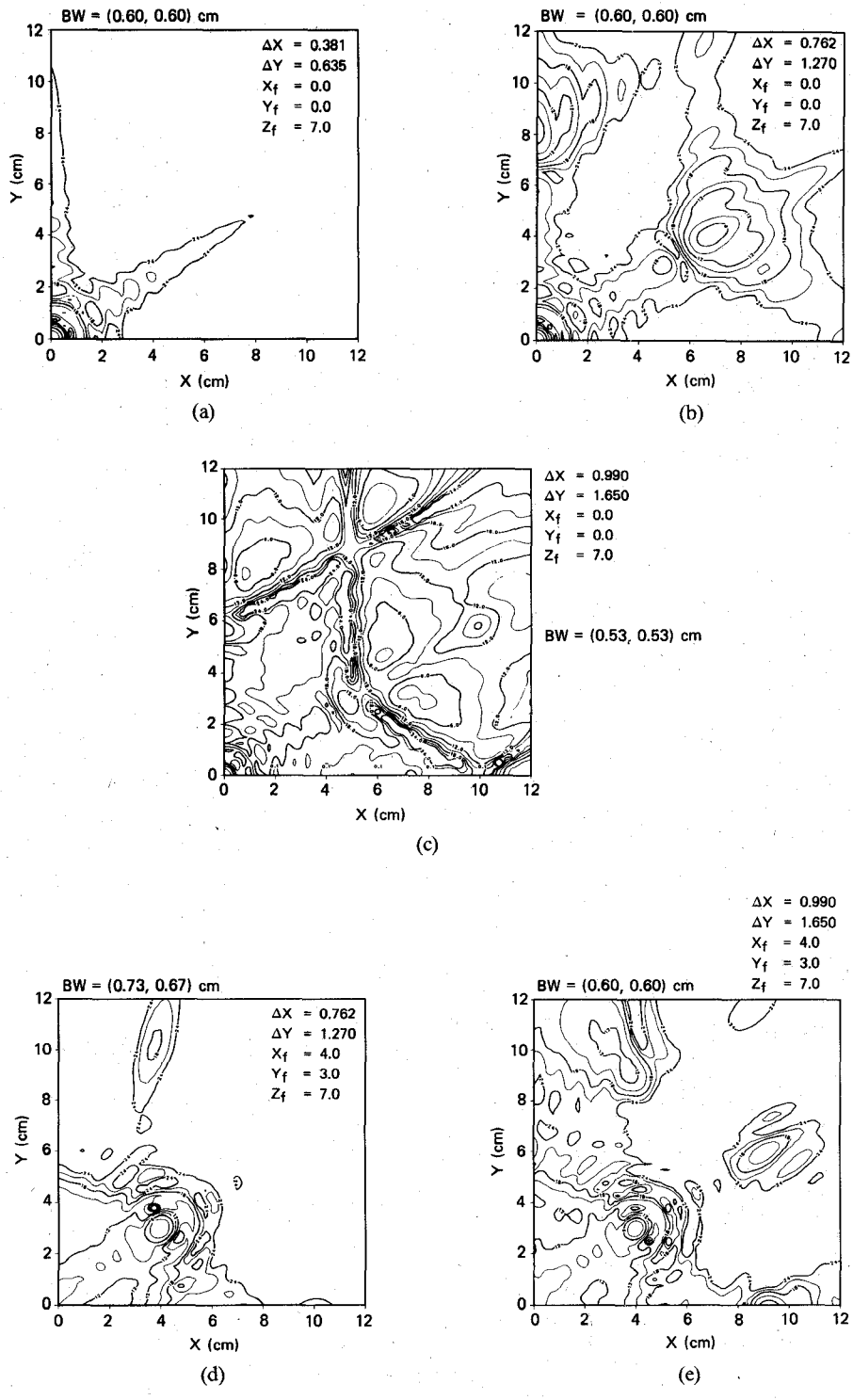

Fig. 4. Amplitude contours in isodecibels for constant $Z_f = 7.0$.

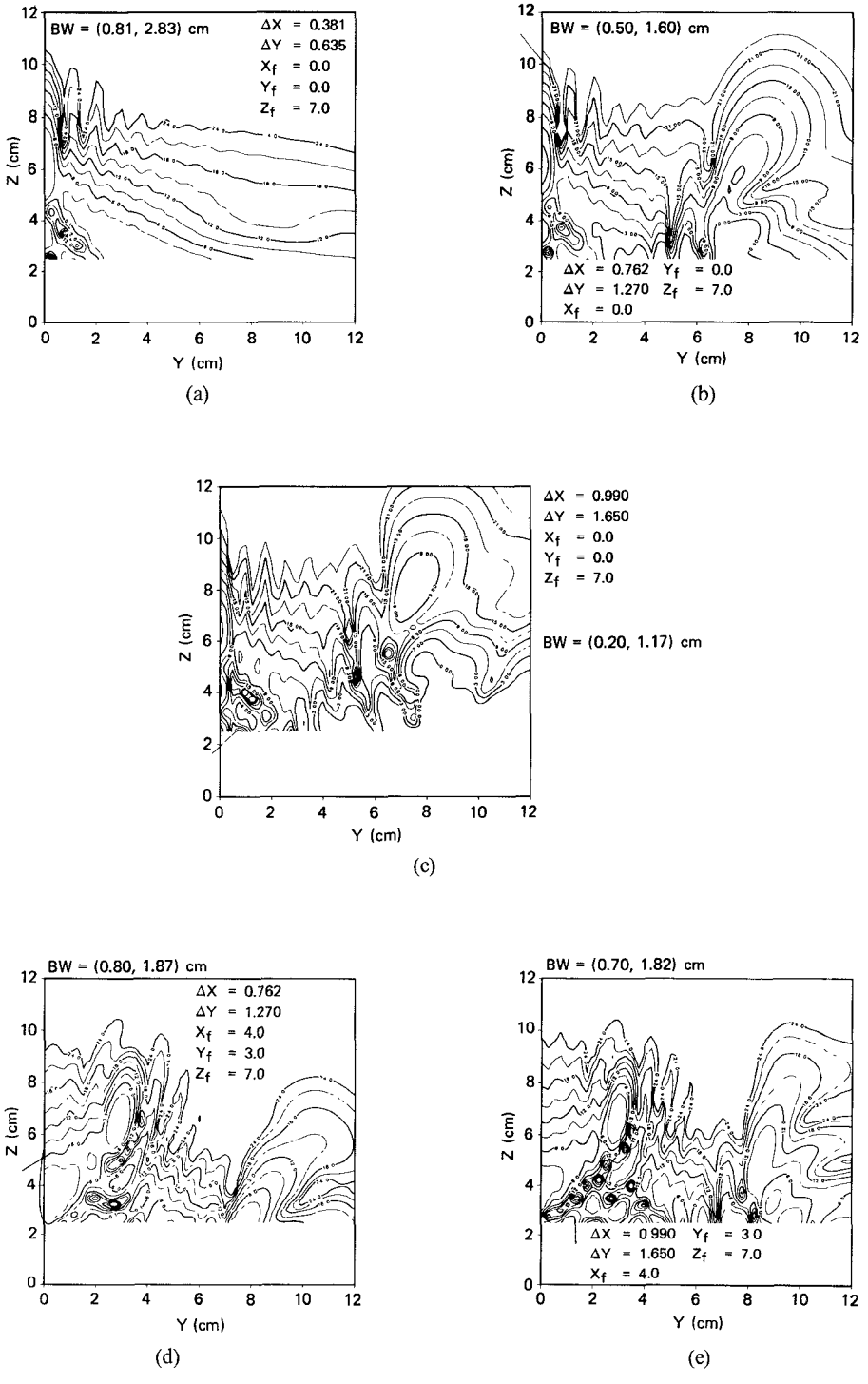

Fig. 5. Amplitude contours in isodecibels for constant X_f.

TABLE I
ARRAY BEAM CHARACTERISTICS OF THE FIELD PATTERNS AT 3 GHz

FOCAL POINT (x y z) cm	ELEMENT SPACING (dx dy) cm	PEAK AT Z=7 (x y z) cm	PEAK AT $X=X_f$ (x y z) cm	BEAMWIDTH AT Z=7 (dx dy) cm	BEAMWIDTH AT $X=X_f$ (dy dz) cm
0 0 7	.381 .635	0 0 7	0 0 6	.60 .60	.81 2.83
0 0 7	.762 1.27	0 0 7	0 0 6	.60 .60	.50 1.60
0 0 7	.990 1.65	0 0 7	0 0 6.5	.53 .53	.20 1.17
4 3 7	.762 1.27	4 3 7	4 2.75 6.25	.74 .67	.80 1.87
4 3 7	.900 1.65	4 3 7	4 3 6.5	.60 .60	.70 1.82

1) Using the method of phase and amplitude conjugations, one may achieve a satisfactory degree of three-dimensional focusing in the neighborhood of radiation sources in a lattice structure. There is a slight shift of the peak point of the field from the intended focal point as defined in the phase–amplitude conjugation factor. The shift, as outlined in Table I, generally points toward the center of the array. This should not pose any problem for practical applications since it can be calibrated.

2) Upon applying the phase and amplitude conjugations, the field patterns and the beam characteristics in the transverse direction appear to have similar dependency upon the lattice structure and the array size as that of a Fraunhofer field. Thus, the transverse beamwidth becomes narrower as the element spacing increases, at the expense of more grating lobes. Interestingly, this behavior also applies to the longitudinal beamwidth. Therefore, for a small target, it is possible to improve the resolution further by increasing the element spacing, as long as the target does not extend to the region covered by grating lobes.

3) Along the longitudinal direction, the field patterns and the beam characteristics using the phase and amplitude conjugations differ considerably from that of a Fraunhofer field. A Fraunhofer field is invariant in the longitudinal direction, except for the inverse-square dependence, whereas a local field under phase and amplitude conjugations has a diffraction structure in the longitudinal direction, as well as in the transverse direction. Therefore, some degree of focusing of the local field along the longitudinal direction may be achieved using the phase and amplitude conjugation technique. It must be remarked that, as the axial distance increases, the sensitivity of longitudinal focusing to the phase–amplitude conjugation decreases. Our analysis of the field pattern for focusing at 30-cm axial distance indicates that the conjugation factor is totally overcome by the exponential attenuation. However, the transverse focusing remains good even at this axial distance.

REFERENCES

[1] A. S. Pressman, *Electromagnetic Fields and Life*. New York: Plenum, 1970.

[2] L. E. Larsen and J. H. Jacobi, "Microwave scattering parameter imagery of an isolated canine kidney," *Med. Phys.*, vol. 6, pp. 394–402, 1979.

[3] J. H. Jacobi, L. E. Larsen, and C. T. Hast, "Water-immersed microwave antennas and their application to microwave interrogation of biological targets," *IEEE Trans. Microwave Theory Tech.*, vol. MTT-27, pp. 70–78, 1979.

[4] J. H. Bolomey, A. Izadnegahdar, L. Jofre, Ch. Pichot, G. Peronnet, and M. Solaimani, "Microwave diffraction tomography for biomedical applications," *IEEE Trans. Microwave Theory Tech.*, vol. MTT-30, pp. 1998–2000, 1982.

[5] N. H. Farhat, D. L. Jaggard, T. H. Chu, D. B. Ge, and S. Mankoff, presented at the 3rd Ann. Benjamin Franklin Sym. on Advances in Antennas and Microwave Technology, Philadelphia, PA, 1983.

[6] L. E. Larsen and J. H. Jacobi, "Methods of microwave imagery for diagnostic application," *Diagnostic Imaging in Medicine*, NATO Advanced Science Institute Series E, no. 61, C. R. Reba, Ed. The Hague: Nijhoff, 1983, pp. 68–123.

[7] T. C. Guo, W. W. Guo, and L. E. Larsen, "Comment on 'Microwave diffraction tomography for biomedical applications'," *IEEE Trans. Microwave Theory and Tech.*, vol. MTT-32, pp. 473–474, Apr. 1984.

[8] _____, in *Proc. IEEE 8th Int. Conf. on Infrared and Millimeter Waves*, Miami Beach, FL, Dec. 12–17, 1983.

[9] M. Melek and A. P. Anderson, "Theoretical studies of localized tumour heating using focused microwave arrays," *Inst. Elec. Eng. Proc.*, vol. 127, Pt F, no. 4, pp. 319–321, 1980.

[10] J. Mendecki, E. Friedenthal, and C. Botstein, "Microwave-induced hyperthermia in cancer treatment: apparatus and preliminary results," *Int. J. Radiation Oncology Biol. Phys.*, vol. 4, no. 11, pp. 1095–1103, 1978.

[11] D. A. Christensen and C. H. Durney, "Hyperthermia production for cancer therapy: A review of fundamentals and methods," *J. Microwave Power*, vol. 16, no. 2, June 1981.

[12] I. Yamaura, "Measurements of 1.8–2.7 GHz microwave attenuation in the human torso," *IEEE Trans. Microwave Theory Tech.*, vol. MTT-25, pp. 707–710, 1977.

[13] J. H. Jacobi and L. E. Larsen, "Microwave time delay spectroscopic imagery of isolated canine kidney," *Med. Phys.*, vol. 7, no. 1. pp. 1–7, 1980.

[14] H. P. Schwan, "Radiation biology, medical applications, and radiation hazards," in *Microwave Power Eng.*, vol. 2, E. C. Okress, Ed. New York: Academic, 1968, pp. 215–232.

[15] K. Kurokawa, "Electromagnetic wave and waveguides with wall impedance," *IEEE Trans. Microwave Theory Tech.*, vol. MTT-13, pp. 314–320, 1962.

[16] J. Jackson, *Classical Electrodynamics*. New York: Wiley, 1962, ch. 9.

Theodore C. Guo (SM'77) received the B.S. degree in physics from Chung-Yuan College of Sciences and Engineering, Taiwan, in 1963, and

a Ph.D. degree in physics from the University of Denver, CO, in 1971.

He was a Research Associate and a Physics Instructor at the University of Denver from 1971 until March 1973, when he joined the University of Brussels and the International (Solvay) Institute of Physics and Chemistry, Brussels, Belgium, where he was engaged in the basic research in irreversible thermodynamics and nonequilibrium statistical mechanics. He returned to the United States at the end of 1976 to join Tracor, Inc., as a Senior Scientist in its Rockville Laboratory, MD, and directed the Research and Development in quantum optics and fiber optics. From 1978 to 1983, he was with IIT Research Institute, Annapolis, MD, where he was engaged in basic and applied research of quantum electronics, nonsteady state physics and irreversible thermodynamics, transient dielectric interactions, and microwave medical physics. Since February 1983, he has been with the Johns Hopkins University Applied Physics Laboratory Laurel, MD, and has continued the research in these subjects.

✤

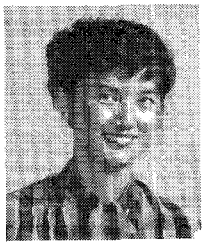

Wendy W. Guo (SM'79) graduated from Chung-Yuan College of Sciences and Engineering, Taiwan, in 1968 with a B.S. degree in chemistry, and received the M.S. and Ph.D. degrees in physics from the University of Denver, CO, in 1970 and 1973, respectively.

Between 1973 and 1976, she was a Research Physicist in the University of Brussels and International (Solvay) Institute of Physics and Chemistry, Brussels, Belgium, where she was involved in the basic research of irreversible thermodynamics and nonequilibrium statistical physics. From 1976 to 1978, she was a Senior Scientist in Tracor, Inc., Rochville, MD. From 1978 to 1983, she was a Senior Research Engineer in IIT Research Institute, Annapolis, MD, where she was engaged in a number of projects concerning basic and applied research of transient dielectric interactions in condensed matters and nonsteady-state physics, microwave interaction in biological systems, electromagnetic theory, and adaptive array and radar analysis. Since February 1983, she has been with the Applied Physics Laboratory, Johns Hopkins University, Laurel, MD, where she has beeen performing research in thermodynamics and statistical physics with respect to the transient state interaction of radiation and matter, thermal properties of microwave interaction with biological materials, and application of microwave physics in medicine.

✤

Lawrence Edwin Larsen (M'81–SM'82) attended and received the M.D. degree magna cum laude from the University of Colorado, Fort Collins, in 1968. He was awarded an NIH postdoctoral fellowship in biophysics at UCLA for the period 1968–1970.

He then served in the United States Army as a Research Physiologist in the Department of Microwave Research at the Walter Reed Army Institute of Research during 1970–1973. From 1973 to 1975, he accepted a faculty appointment in the Radiology Department at the Baylor College of Medicine in Houston, TX, where he taught physiology and computer sciences. In 1975, he returned to the Walter Reed Army Institute of Research as the Associate Chief of Microwave Research. He was appointed the Department Chief in 1977 and presently serves in that role with the rank of Colonel, Medical Corps. He holds several patents.

Microwave Thermoelastic Tissue Imaging—System Design

JAMES C. LIN, SENIOR MEMBER, IEEE, AND KAREN H. CHAN

Abstract—**A microwave-induced thermoelastic tissue imaging system is proposed as a new and promising imaging modality. It possesses unique features that permit noninvasive imaging of tissue characteristics which are not identifiable by other techniques. It uses nonionizing radiation and relies on a beam of impinging microwave energy to launch an acoustic wavefront into tissue. This thermoelastic wave of pressure propagates through the tissue and is detected by a two-dimensional array of piezoelectric transducers positioned on the body surface to give an image of the intervening tissue structure. Signals from the output of this transducer array are amplified and band-limited. A computer-controlled data acquisition system samples and converts them to digital form for further processing. A hybrid parallel/serial design for dividing the array into segments and collecting data from each segment sequentially is used. The area image sensor offers inherent geometric stability essential for reliable measurement. Error in scan position is not a concern, since mechanical scanning is not involved. The gray level resolution is 256 after digitization, and the spatial resolution is 5×5 mm. These resolutions, along with a calculated signal-to-noise ratio greater than 2500, are sufficient to provide structural information needed to render microwave-induced thermoelastic imaging a useful, noninvasive method for imaging biological tissues.**

Manuscript received October 12, 1983; revised March 11, 1984. This work was supported in part by the National Science Foundation and the Office of Naval Research.

The authors are with the Department of Bioengineering, University of Illinois at Chicago, P.O. Box 4348, Chicago, IL 60680.

I. Introduction

THE LAST DECADE has witnessed tremendous advances in the field of biomedical imaging. Imaging modalities and protocols which only a short time ago were in the experimental stage have, during the last decade, become routine clinical procedures. In hematology, for example, automated instruments process blood slides on a daily basis in the clinical laboratory. In nuclear medicine, nuclear image processors are used in perform over 7 million scintigraphic studies yearly in the U.S. In cardiology, real-time ultrasonic systems are used routinely to image

0018-9480/84/0800-0854$01.00 ©1984 IEEE